Journal of Solid Mechanics Vol. 6, No. 4 (2014) pp. 347-365

Influence of the Elastic Foundation on the Free Vibration and Buckling of Thin-Walled Piezoelectric-Based FGM Cylindrical Shells Under Combined Loadings

M. Mohammadimehr*, M. Moradi, A. Loghman

Department of Solid Mechanics, Faculty of Mechanical Engineering, University of Kashan, Kashan, Iran

Received 19 June 2014; accepted 25 August 2014

ABSTRACT

In this paper, the influence of the elastic foundation on the free vibration and buckling of thin-walled piezoelectric-based functionally graded materials (FGM) cylindrical shells under combined loadings is investigated. The equations of motion are obtained by using the principle of Hamilton and Maxwell's equations and the Navier's type solution used to solve these equations. Material properties are changed according to power law in the direction of thickness. In this study, the effects of Pasternak elastic foundation coefficients and also the effects of material distribution, geometrical ratios and loading conditions on the natural frequencies are studied. It is observed that by increasing Pasternak elastic medium coefficients, the natural frequencies of functionally graded piezoelectric materials (FGPM) cylindrical shell always increases. The mode shapes of FGPM cylindrical shell has been shown in this research and the results show that the distribution of the radial displacements is more significant than circumferential and longitudinal displacements.

Keywords: Buckling; Free vibration; Elastic foundation; Mode shapes; Thin-walled cylindrical shell; FGPM.

1 INTRODUCTION

In the past two decades, researchers are always looking for materials that their properties can be optimized according to the working conditions, so functionally graded piezoelectric materials (FGPM) have been the subject of many investigations. At first in 1984, the idea of producing this materials was proposed by Japanese scientists Yamanouchi et al. [1] and Koizumi [2]. FGPM used the benefits of functional graded materials (FGM) and piezoelectric materials together. The unique characteristic of these materials is that their microstructure varies in the thickness direction and by applying a potential difference their shape is changed and vice versa, also the high thermal resistance of these materials makes them a good choice for high temperature working condition. Today these materials are widely used in the electrical and electromechanical devices such as sensors, actuators and in airspace industries including airplane flaps and so on.

Investigating free vibrations of thin-walled cylindrical shells made of FGPM is crucial in theoretical and practical aspects. To reach a real model, we should consider the interaction of cylindrical shells and surrounded medium with an appropriate model, the Pasternak model is a good choice for this purpose by Pasternak [3].

* Corresponding author. Tel.: +98 31 55912423; Fax: +98 31 55912424.
E-mail address: mmohammadimehr@kashanu.ac.ir (M. Mohammadimehr).

At first, Loy et al. [4] investigated the effects of material distribution in thickness direction on the free vibrations of functionally graded thin-walled cylindrical shell. Pradhan and co-workers [5] studied the vibration characteristics of functionally graded cylindrical shells under various boundary conditions. Najafizadeh and Isvandzibaei [6] presented a model for vibration of functionally graded cylindrical shells based on higher order shear deformation plate theory with ring support. In these three mentioned works, the Rayleigh-Ritz method is used to obtain the constitutive equations of thin cylindrical shells. Shah et al. [7] illustrated the vibrations of functionally graded cylindrical shells based on Winkler and Pasternak foundations, which wave propagation method is used to solve dynamic equations in cylindrical shells. Bhangale and Ganesan [8] simulated the free vibration of a simply supported non-homogeneous functionally graded cylindrical shell in magneto-electro-elastic fields using finite element method. Their results discovered the effects of magneto-electro fields and geometric parameters on natural frequency. Kadoli and Ganesan [9] studied the buckling and free vibration analysis of functionally graded cylindrical shells subjected to a temperature-specified boundary condition. According to numerical results of this work in high temperature working condition, the natural frequencies are decreased dramatically.

Malekzadeh and Heydarpour [10] considered the free vibration of rotating functionally graded cylindrical shells subjected to thermal environment based on the first order shear deformation theory (FSDT) of cylindrical shells. They applied the differential quadrature method (DQM) to discretize the thermoelastic equilibrium equations and the equations of motion. Ebrahimi and Najafizadeh [11] analyzed the free vibration of a two-dimensional functionally graded circular cylindrical shell. Their results showed that the natural frequency of the material can be modified in order to meet the expected results through manipulation of the constituent volume fractions. Sheng and Wang [12] presented an analytical method for functionally graded cylindrical shells based on Hamilton's principle, von Karman's non-linear theory and the FSDT, and subjected to thermal and axial loadings. Du and Li [13] investigated the nonlinear vibrations of functionally graded cylindrical shells in thermal environments. In this work, the effects of temperature change and volume fractions of constituent material on the amplitude response of the system are discussed. Sofiyev and Kuruoglu [14] studied the torsional vibration and buckling analysis of cylindrical shell with functionally graded coatings surrounded by an elastic medium. They used a Pasternak foundation model to describe the shell–foundation interaction and derived the basic equations and solved using Galerkin method. Sheng and Wang [15] applied the analytical method for smart functionally graded laminated cylindrical shells with thin piezoelectric layers based on Hamilton's principle and von Karman's nonlinear theory. They solved the coupled nonlinear equations of motion by the Runge–Kutta numerical method. Rafiee et al. [16] presented the nonlinear vibration and dynamic response of the simply supported piezoelectric functionally graded material shells under combined electrical, thermal, mechanical and aerodynamic loadings. They obtained the influences of the shell geometry and piezoelectric thickness, temperature change, external constant electric voltage on the nonlinear dynamic behavior of the piezoelectric functionally graded shells in details. Ghorbanpour Arani et al. [17] presented electro-magneto-mechanical responses of a radially polarized rotating shaft made from FGPM and subjected to a uniform magnetic field with mechanical loads and electric potentials. They derived exact solutions for electric displacement, stresses, electric potentials, and perturbation of the magnetic field vector using the infinitesimal theory of electro-magneto-elasticity. Their numerical results showed that the responses were strongly affected by power law index B.

Motivated by these considerations, we aim to investigate the Winkler and Pasternak foundation effects on free vibration and buckling analysis of cylindrical shells under combination of electric, thermal and mechanical loadings. Also, in this research, mode shapes of FGPM cylindrical shells have been illustrated. Moreover, the properties of the FGPM cylinder are assumed to vary as a power function in the thickness direction. The governing equations of motion are obtained by using Hamilton's principle and Maxwell's equation. A Navier's type solution is presented to solve the governing equations of motion.

2 MATHEMATICAL MODEL AND CONSTITUTIVE EQUATIONS

Fig. 1 shows a thin-walled piezoelectric-based FGM cylindrical shell which surrounded by a Pasternak foundation. Geometry parameters such as R, h, and L are the mean radius, thickness, and length of cylindrical shell, respectively. In this work, the cylindrical shell polarized in thickness direction. In Fig. 1, the cylindrical coordinate z, θ, x denote the radial, circumferential, and longitudinal axes, respectively. The components of displacement vector in cylindrical coordinate x, ϑ, and z are shown by u, v, and w, respectively.

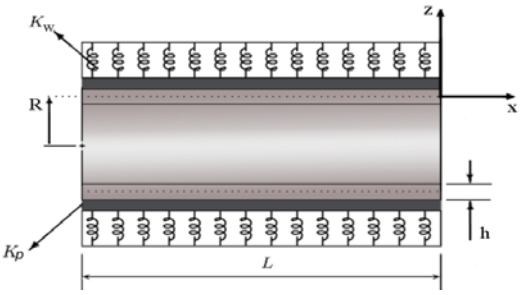

Fig. 1
A schematic of thin-walled FGPM cylindrical shell which surrounded by a Winkler and Pasternak foundation in the cylindrical coordinate z, θ, x .

The properties of FGPM are assumed to be a function of z in thickness direction as follows:

$$C_{ij} = C_{ij}(z), \quad e_{ij} = e_{ij}(z), \quad \zeta_{ij} = \zeta_{ij}(z), \quad k = k(z), \qquad P_i = P_i(z), \qquad \rho = \rho(z), \quad \alpha_{ij} = \alpha_{ij}(z) \tag{1}$$

In which C_{ij}, e_{ij} and ζ_{ij} are elastic, piezoelectric, and dielectric constants, respectively. Also k, P_i, ρ and α_{ij} are the thermal coefficients, pyroelectric constants, density, and thermal expansion coefficients, respectively.The material properties vary between the inner and outer surface of FGPM cylindrical shell according to the following power function:

$$F(z) = F_i + (F_o - F_i)\cdot\left(\frac{z}{h} + \frac{1}{2}\right)^{\beta} \qquad \left(0 \le \beta \le \infty\right), \tag{2}$$

In which F_i and F_o are the properties of the inner and outer surfaces of cylindrical shell, respectively, and β is a power of volume fraction.

For steady-state conditions with no heat generation, the appropriate form of the heat equation in radial (thickness) direction yields [18]:

$$\frac{1}{z}\cdot\left(z\cdot K(z)\cdot T'(z)\right)' = 0, \quad \left(-\frac{h}{2} \le z \le \frac{h}{2}\right) \tag{3}$$

Considering steady temperature conditions on the inner and outer surfaces of cylinder, the following equation is obtained:

$$T(z) = T_i - \frac{T_{io}}{\int_{-\frac{h}{2}}^{\frac{h}{2}} \frac{dz}{K(z)\cdot z}} \cdot \int_{-\frac{h}{2}}^{z} \frac{dz}{K(z)\cdot z}, \tag{4}$$

In the Eq. (4), T_{io} is temperature change between the inner and outer surfaces of cylindrical shell, $T_{io} = T_i - T_o$.

According to plane stress assumption , the normal stress equals to zero. The constitutive equations of a piezoelectric cylindrical shell are shown in the following form [19]:

$$\begin{Bmatrix} \sigma_x \\ \sigma_\theta \\ \tau_{x\theta} \\ \tau_{\theta z} \\ \tau_{xz} \end{Bmatrix} = \begin{bmatrix} C_{11e} & C_{12e} & 0 & 0 & 0 \\ C_{12e} & C_{22e} & 0 & 0 & 0 \\ 0 & 0 & C_{66e} & 0 & 0 \\ 0 & 0 & 0 & C_{44e} & 0 \\ 0 & 0 & 0 & 0 & C_{55e} \end{bmatrix} \cdot \begin{Bmatrix} \varepsilon_x \\ \varepsilon_\theta \\ \gamma_{x\theta} \\ \gamma_{\theta z} \\ \gamma_{xz} \end{Bmatrix} - \begin{Bmatrix} \alpha_{11e} \\ \alpha_{22e} \\ 0 \\ 0 \\ 0 \end{Bmatrix} \cdot T - \begin{bmatrix} 0 & 0 & e_{31e} \\ 0 & 0 & e_{32e} \\ 0 & 0 & 0 \\ 0 & e_{24e} & 0 \\ e_{15e} & 0 & 0 \end{bmatrix} \cdot \begin{Bmatrix} E_x \\ E_\theta \\ E_z \end{Bmatrix} \tag{5a}$$

$$\begin{Bmatrix} D_x \\ D_\theta \\ D_z \end{Bmatrix} = \begin{bmatrix} 0 & 0 & 0 & 0 & e_{15e} \\ 0 & 0 & 0 & e_{24e} & 0 \\ e_{31e} & e_{32e} & 0 & 0 & 0 \end{bmatrix} \cdot \begin{Bmatrix} \varepsilon_x \\ \varepsilon_\theta \\ \gamma_{x\theta} \\ \gamma_{\theta z} \\ \gamma_{xz} \end{Bmatrix} + \begin{Bmatrix} P_{xe} \\ P_{\theta e} \\ P_{ze} \end{Bmatrix} \cdot T + \begin{bmatrix} \zeta_{11e} & 0 & 0 \\ 0 & \zeta_{22e} & 0 \\ 0 & 0 & \zeta_{33e} \end{bmatrix} \cdot \begin{Bmatrix} E_x \\ E_\theta \\ E_z \end{Bmatrix} \tag{5b}$$

where C_{ije}, e_{ije} and ζ_{ije} are the equivalent values of elastic, piezoelectric and dielectric constants, respectively. Also P_{xe}, $P_{\theta e}$ and P_{ze} are the components of equivalent pyroelectric constants, and α_{11e} and α_{22e} are the equivalent thermal expansion coefficients, these equivalent values completely defined in Appendix A. Also $\sigma_x, \sigma_\theta, \tau_{x\theta}, \tau_{\theta z}$ and τ_{xz} are components of the normal and shear stresses, $\varepsilon_x, \varepsilon_\theta, \gamma_{\theta z}, \gamma_{xz}$ and $\gamma_{x\theta}$ denote components of the normal and shear strains, D_x, D_θ and D_z are electrical displacement components and E_x, E_θ and E_z state the electrical field components. Since, the stress in thickness direction is zero. Also, subscript "*e*" shows the equivalent values of properties that are completely defined in Appendix A.

The electrical field intensity in Eqs. (5a) and (5b) is as a function of electrical potential [20]:

$$E_x = -\frac{\partial \varphi(x,\theta,z,t)}{\partial x},\ E_\theta = -\frac{1}{R+z}\frac{\partial \varphi(x,\theta,z,t)}{\partial \theta},\ E_z = -\frac{\partial \varphi(x,\theta,z,t)}{\partial z}, \tag{6}$$

$$\varphi(x,\theta,z,t) = \frac{2z \cdot V(x,\theta,t)}{h} + \left[z^2 - \left(\frac{h}{2}\right)^2 \right] \psi(x,\theta,t), \tag{7}$$

In which $\psi(x,\theta,t), V(x,\theta,t)$, and $\phi(x,\theta,z,t)$ denote the electrical potential distribution in thickness, the electrical potential that imposed on the inner and outer surfaces of the cylindrical shell and the total electrical potential, respectively, also *R* is the mean radius of cylindrical shell. In this work, the direction of polarization is considered along *x*-direction. The linear strain-displacement relations are [21]:

$$\varepsilon_{xx} = u_{,x} \quad , \varepsilon_{\theta\theta} = \left(v_{,\theta} + w\right)/R, \quad \gamma_{x\theta} = u_{,\theta}/R + v_{,x}\ , \quad \gamma_{\theta z} = \phi_\theta + w_{,\theta}/R\ , \quad \gamma_{xz} = \phi_x + w_{,\mathrm{x}}\ , \tag{8}$$

Here, the comma indicates a partial derivative. According to the first-order shear deformation shell theory, the displacement field of the shell is assumed to be [22]:

$$u(\mathrm{x},\theta,\mathrm{z}) = \overline{u}(\mathrm{x},\theta) + \mathrm{z}\cdot\phi_x(x,\theta), \quad \mathrm{v}(\mathrm{x},\theta,\mathrm{z}) = \overline{v}(\mathrm{x},\theta) + \mathrm{z}\cdot\phi_\theta(x,\theta)\ , \quad \mathrm{w}(\mathrm{x},\theta,\mathrm{z}) = \overline{w}(\mathrm{x},\theta)\ , \tag{9}$$

Substituting Eq. (9) into Eq. (8) yields the relationship between general strains and mid surface strains in the following form [21]:

$$\begin{Bmatrix} \varepsilon_x \\ \varepsilon_\theta \\ \gamma_{x\theta} \\ \gamma_{\theta z} \\ \gamma_{xz} \end{Bmatrix} = \begin{Bmatrix} \overline{\varepsilon}_x \\ \overline{\varepsilon}_\theta \\ \overline{\gamma}_{\theta z} \\ \overline{\gamma}_{xz} \\ \overline{\gamma}_{x\theta} \end{Bmatrix} + z \cdot \begin{Bmatrix} \overline{\overline{\varepsilon}}_x \\ \overline{\overline{\varepsilon}}_\theta \\ \overline{\overline{\gamma}}_{\theta z} \\ \overline{\overline{\gamma}}_{xz} \\ \overline{\overline{\gamma}}_{x\theta} \end{Bmatrix}, \tag{10}$$

$$\begin{Bmatrix} \overline{\varepsilon}_x \\ \overline{\varepsilon}_\theta \\ \overline{\gamma}_{\theta z} \\ \overline{\gamma}_{xz} \\ \overline{\gamma}_{x\theta} \end{Bmatrix} = \begin{Bmatrix} \overline{u}_{,x} \\ \left(\overline{v}_{,\theta} + \overline{w}\right)/R \\ \phi_\theta + \overline{w}_{,\theta}/R \\ \phi_x + \overline{w}_{,x} \\ \overline{u}_{,\theta}/R + \overline{v}_{,x} \end{Bmatrix}, \tag{11}$$

$$\begin{Bmatrix} \overline{\overline{\varepsilon}}_x \\ \overline{\overline{\varepsilon}}_\theta \\ \overline{\overline{\gamma}}_{\theta z} \\ \overline{\overline{\gamma}}_{xz} \\ \overline{\overline{\gamma}}_{x\theta} \end{Bmatrix} = \begin{Bmatrix} \phi_{x,x} \\ \phi_{\theta,\theta}/R \\ 0 \\ 0 \\ \phi_{\theta,x} + \phi_{x,\theta}/R \end{Bmatrix}, \tag{12}$$

The resultant forces, moments, and shears can be defined as follows:

$$\begin{aligned} &\left\{N_x, N_\theta, N_{x\theta}\right\} = \int_{-\frac{h}{2}}^{\frac{h}{2}} \left\{\sigma_x, \sigma_\theta, \sigma_{x\theta}\right\} dz, \quad \left\{M_x, M_\theta, M_{x\theta}\right\} = \int_{-\frac{h}{2}}^{\frac{h}{2}} z \cdot \left\{\sigma_x, \sigma_\theta, \sigma_{x\theta}\right\} dz, \\ &\left\{Q_x, Q_\theta\right\} = k_s \int_{-\frac{h}{2}}^{\frac{h}{2}} \left\{\tau_{xz}, \tau_{\theta z}\right\} dz, \end{aligned} \tag{13}$$

Here, k_s is the shear correction factor and is equal to $\pi^2/12$ [23]. Hamilton's principle is used to minimize the Lagrangian (L) of the deformed cylindrical shell, so the equations of motion for the FGPM thin-walled cylindrical shells surrounded by the Pasternak elastic foundation under combined loadings are obtained as [24, 25]:

$$\delta L = \int_0^t \left(\delta K - \delta U - \delta V_N - \delta V_f\right) dt = 0, \tag{14}$$

In which K, U, and V_N are the kinematic, strain, and potential energies of system, respectively, and V_f is the energy from elastic foundation forces and defined as follows [19]:

$$\begin{aligned} &K = \frac{1}{2}\int_s \left[\int_{-\frac{h}{2}}^{\frac{h}{2}} \rho\left(\dot{u}^2 + \dot{v}^2 + \dot{w}^2\right) R dz\right] d\theta dx, \quad U = \frac{1}{2}\int_s \left[\int_{-\frac{h}{2}}^{\frac{h}{2}} \left(\left\{\sigma\right\}^T \left\{\varepsilon\right\} - \left\{D\right\}^T \left\{E\right\}\right) R dz\right] d\theta dx, \\ &V_N = \frac{1}{2}\int_s \left[\left(N_0 - N_x^T - N_x^p\right)\left(\frac{\partial w}{\partial x}\right)^2\right] R d\theta dx + \frac{1}{2}\int_s \left[\left(N_0 - N_x^T - N_x^p\right)\left(\frac{\partial v}{\partial x}\right)^2\right] R d\theta dx, \\ &V_f = \frac{1}{2}\int_s \left[K_w w^2 + K_p\left(\left(\frac{\partial w}{\partial x}\right)^2 + \frac{1}{R^2}\left(\frac{\partial w}{\partial \theta}\right)^2\right)\right] R\, d\theta\, dx, \end{aligned} \tag{15}$$

Here N_0, N_x^T and N_x^p are the mechanical, thermal, and electrical loadings in the axial direction, respectively, and are defined in Appendix B, are also K_w and K_p are Winkler and Pasternak coefficients. Substituting Eqs. (6), (7), and (10) into Eq. (14), the equations of motion for FGPM thin-walled cylindrical shell under electrical, thermal, and mechanical loadings with considering elastic foundation is expressed in the following form:

$$\delta u: \frac{\partial N_x}{\partial x}+\frac{1}{R}\frac{\partial N_{x\theta}}{\partial \theta}=I_1\,\ddot{u}+I_2\,\ddot{\phi}_x,\quad \delta v: \frac{\partial N_{x\theta}}{\partial x}+\frac{1}{R}\frac{\partial N_\theta}{\partial \theta}+\frac{1}{R}Q_\theta+\left(N_0-N_x^T+N_x^P\right)\frac{\partial^2 v}{\partial x^2}=I_1\,\ddot{u}+I_2\,\ddot{\phi}_x,$$
$$\delta w: \frac{\partial Q_x}{\partial x}+\frac{1}{R}\frac{\partial Q_\theta}{\partial \theta}-\frac{1}{R}N_\theta+\left(N_0-N_x^T+N_x^P\right)\frac{\partial^2 w}{\partial x^2}-k_w\cdot w+k_p\cdot\left(\frac{\partial^2 w}{\partial x^2}+\frac{1}{R^2}\frac{\partial^2 w}{\partial \theta^2}\right)=I_1\cdot\ddot{w}, \tag{16}$$
$$\delta\phi_x: \frac{\partial M_x}{\partial x}+\frac{1}{R}\frac{\partial M_{x\theta}}{\partial \theta}-Q_x=I_2\,\ddot{u}+I_3\,\ddot{\phi}_x,\quad \delta\phi_\theta: \frac{\partial M_{x\theta}}{\partial x}+\frac{1}{R}\frac{\partial M_\theta}{\partial \theta}-Q_\theta=I_2\,\ddot{v}+I_3\,\ddot{\phi}_\theta,$$

In Eq. (16), the mass inertia is defined as follows:

$$\left\{I_1,I_2,I_3\right\}=\int_{-\frac{h}{2}}^{\frac{h}{2}}\rho\cdot\left\{1,z,z^2\right\}dz \tag{17}$$

Substituting Eqs. (5), (13) and (17) into Eq. (16), the governing equations of motion for the thin-walled piezoelectric-based FGM cylindrical shell can be rewritten:

$$\begin{aligned}
&B_{11}\,u+B_{12}\,v+B_{13}\,w+B_{14}\,\phi_x++B_{15}\phi_\theta+B_{16}\psi+B_1=I_1\,\ddot{u}+I_2\,\ddot{\phi}_x,\\
&B_{21}\,u+B_{22}\,v+B_{23}\,w+B_{24}\,\phi_x+B_{25}\,\phi_\theta+B_{26}\,\psi+B_2+=I_1\,\ddot{v}+I_2\ddot{\phi}_\theta,\\
&B_{31}\,u+B_{32}\,v+B_{33}\,w+B_{34}\,\phi_x+B_{35}\,\phi_\theta+B_{36}\,\psi+B_3=I_1\,\ddot{w},\\
&B_{41}u+B_{42}v+B_{43}w+B_{44}\phi_x+B_{45}\phi_\theta+B_{46}\psi+B_4=I_2\,\ddot{u}+I_3\,\ddot{\phi}_x,\\
&B_{51}\,u+B_{52}\,v+B_{53}\,w+B_{54}\,\phi_x+B_{55}\,\phi_\theta+B_{56}\,\psi+B_5=I_2\,\ddot{v}+I_3\,\ddot{\phi}_\theta,
\end{aligned} \tag{18}$$

The Maxwell's equation can be considered as follows [26]:

$$\int_{-\frac{h}{2}}^{\frac{h}{2}}\left(\frac{\partial D_x}{\partial x}+\frac{1}{R}\frac{\partial D_\theta}{\partial \theta}+\frac{\partial D_z}{\partial z}+\frac{1}{R}D_z\right)dz=0, \tag{19}$$

Substituting Eq. (5) into Eq. (19) yields:

$$B_{61}u+B_{62}v+B_{63}w+B_{64}\phi_x+B_{65}\phi_\theta+B_{66}\psi=B_6 \tag{20}$$

All coefficients $B_{ij}\,(i,j=1,2,...,6)$ in Eqs. (18) and (20) are defined in Appendix B.

Navier's type solution is used to solve the governing equations of motion for FGPM thin-walled cylindrical shell with the simply supported boundary conditions, then the components of displacements in Eqs. (18) and (20) should be considered as follows:

$$\begin{Bmatrix}u(x,\theta,t)\\ v(x,\theta,t)\\ w(x,\theta,t)\\ \phi_x(x,\theta,t)\\ \phi_\theta(x,\theta,t)\\ \psi(x,\theta,t)\end{Bmatrix}=\begin{Bmatrix}u_{mn}(t)\cdot\cos(\lambda_m x)\cdot\cos(n\theta)\\ v_{mn}(t)\cdot\sin(\lambda_m x)\cdot\sin(n\theta)\\ w_{mn}(t)\cdot\sin(\lambda_m x)\cdot\cos(n\theta)\\ \phi_{mn}^x(t)\cdot\cos(\lambda_m x)\cdot\cos(n\theta)\\ \phi_{mn}^\theta(t)\cdot\sin(\lambda_m x)\cdot\sin(n\theta)\\ \psi_{mn}(t)\cdot\sin(\lambda_m x)\cdot\cos(n\theta)\end{Bmatrix}, \tag{21}$$

In which m and n are the half wave numbers in longitudinal and wave numbers in circumferential directions, respectively and $\lambda_m=\frac{m\pi}{L}$. In Eqs. (18) and (20), $B_i\,(i=1,2,...,6)$ is related to the thermal and electrical loadings can be expressed as double Fourier series:

$$\begin{Bmatrix} B_1(x,\theta,t) \\ B_2(x,\theta,t) \\ B_3(x,\theta,t) \\ B_4(x,\theta,t) \\ B_5(x,\theta,t) \\ B_6(x,\theta,t) \end{Bmatrix} = \begin{Bmatrix} B_{mn}^1(t)\cdot\cos(\lambda_m x)\cdot\cos(n\theta) \\ B_{mn}^2(t)\cdot\sin(\lambda_m x)\cdot\sin(n\theta) \\ B_{mn}^3(t)\cdot\sin(\lambda_m x)\cdot\cos(n\theta) \\ B_{mn}^4(t)\cdot\cos(\lambda_m x)\cdot\cos(n\theta) \\ B_{mn}^5(t)\cdot\sin(\lambda_m x)\cdot\sin(n\theta) \\ B_{mn}^6(t)\cdot\sin(\lambda_m x)\cdot\cos(n\theta) \end{Bmatrix}, \tag{22}$$

Substituting Eqs. (21) and (22) into Eqs. (18) and (20) yields:

$$\begin{bmatrix} I_1 & 0 & 0 & I_2 & 0 \\ 0 & I_1 & 0 & 0 & I_2 \\ 0 & 0 & I_1 & 0 & 0 \\ I_2 & 0 & 0 & I_3 & 0 \\ 0 & I_2 & 0 & 0 & I_3 \end{bmatrix} \cdot \begin{Bmatrix} \ddot{u}_{mn} \\ \ddot{v}_{mn} \\ \ddot{w}_{mn} \\ \ddot{\phi}_{mn}^x \\ \ddot{\phi}_{mn}^\theta \end{Bmatrix} + \begin{bmatrix} T_{11} & T_{12} & T_{13} & T_{14} & T_{15} & T_{16} \\ T_{21} & T_{22} & T_{23} & T_{24} & T_{25} & T_{26} \\ T_{31} & T_{32} & T_{33} & T_{34} & T_{35} & T_{36} \\ T_{41} & T_{42} & T_{43} & T_{44} & T_{45} & T_{46} \\ T_{51} & T_{52} & T_{53} & T_{54} & T_{55} & T_{56} \end{bmatrix} \cdot \begin{Bmatrix} u_{mn} \\ v_{mn} \\ w_{mn} \\ \phi_{mn}^x \\ \phi_{mn}^\theta \end{Bmatrix} = \begin{Bmatrix} B_{mn}^1(t) \\ B_{mn}^2(t) \\ B_{mn}^3(t) \\ B_{mn}^4(t) \\ B_{mn}^5(t) \end{Bmatrix} \tag{23}$$

$$T_{61}u_{mn} + T_{62}v_{mn} + T_{63}w_{mn} + T_{64}\phi_{mn}^x + T_{65}\phi_{mn}^\theta + T_{66}\psi_{mn} = L_{mn}^6(t), \tag{24}$$

Coefficients T_{ij} are defined in Appendix C. Using Eq. (24), the electrical potential distribution can be written as follows:

$$\psi_{mn} = \frac{L_{mn}^6(t)}{T_{66}} - \frac{1}{T_{66}}\left(T_{61}\,u_{mn} + T_{62}\,v_{mn}T_{63}\;w_{mn} + T_{64}\;\phi_{mn}^x + T_{65}\;\phi_{mn}^\theta\right), \tag{25}$$

Substituting Eq. (25) into Eq. (23), the governing equations of motion for FGPM cylindrical shell is rewritten as:

$$[M]\cdot\{\ddot{s}\} + [K]\cdot\{s\} = \{F\}, \tag{26}$$

where *F, M* and *K* are the external loadings vector, mass, and stiffness matrices of FGPM cylindrical shell, respectively.

3 FREE VIBRATION OF FGPM CYLINDRICAL SHELLS CONSIDERNG PASTERNAK FOUNDATION

To obtain the natural frequencies and mode shapes, the homogenous solution of Eq. (26) have been considered. For this purpose, the external loadings vector $\{F\}$ is considered to be zero,

$$[M]\cdot\{\ddot{s}\} + [K]\cdot\{s\} = \{0\}, \quad [M] = \begin{bmatrix} I_1 & 0 & 0 & I_2 & 0 \\ 0 & I_1 & 0 & 0 & I_2 \\ 0 & 0 & I_1 & 0 & 0 \\ I_2 & 0 & 0 & I_3 & 0 \\ 0 & I_2 & 0 & 0 & I_3 \end{bmatrix}, \; \{s\} = \begin{Bmatrix} u_{mn}(t) \\ v_{mn}(t) \\ w_{mn}(t) \\ \phi_{mn}^x(t) \\ \phi_{mn}^\theta(t) \end{Bmatrix}, \tag{27}$$

$$[K] = [K_{11}] - N_0[K]_N - T_{io}[K]_T - \Delta V[K]_V - \frac{1}{K_{22}}\{K_{12}\}[K_{21}],$$

where N_0, T_{io}, ΔV are the axial force, temperature change, and potential difference between the inner and outer surfaces, respectively. Also, the other components of Eq. (26) and Eq. (27) are defined in Appendix D.

The solution of Eq. (27) is analytical and their displacements are in the following form:

$$\begin{Bmatrix} u_{mn}(t) \\ v_{mn}(t) \\ w_{mn}(t) \\ \phi_{mn}^{x}(t) \\ \phi_{mn}^{\theta}(t) \end{Bmatrix} = \begin{Bmatrix} u_{mn}^{0} \\ v_{mn}^{0} \\ w_{mn}^{0} \\ \phi_{mn}^{x0} \\ \phi_{mn}^{\theta 0} \end{Bmatrix} \cdot e^{i\omega t} \tag{28}$$

Substituting Eq. (28) into Eq. (27), the eigenvalue equations are obtained as follows:

$$\left([K]-\omega^2[M]\right)\cdot\{s^0\}=\{0\}, \quad \{s^0\}=\left\{u_{mn}^0 \quad v_{mn}^0 \quad w_{mn}^0 \quad \phi_{mn}^{x0} \quad \phi_{mn}^{\theta 0}\right\}^T \tag{29}$$

The natural frequencies and mode shapes of FGPM thin-walled cylindrical shell under thermal, electrical fields and axial loadings is achieved by solving the eigenvalue Eq. (29).

4 BUCKLING ANALYSIS OF FGPM CYLINDRICAL SHELLS WITH PASTERNAK FOUNDATION

For buckling analysis, when the temperature change (T_{io}) and the voltage difference (ΔV) between the inner and outer surfaces are known, in Eq. (29) the natural frequency (ω) vanishes and the static buckling load N_{cr} of the FGPM cylindrical shell with Pasternak foundation can be stated as the following eigenvalue problem:

$$\left([K1]-N_{cr}\cdot[K]_N\right)\cdot\{s^0\}=\{0\}, \tag{30}$$

where

$$[K1]=[K_{11}]-T_{io}[K]_T-\Delta V[K]_V-\frac{1}{K_{22}}\{K_{12}\}[K_{21}], \tag{31}$$

Eq. (30) is used to determine the critical buckling load N_{cr} for different geometry parameters and buckling modes m and n.

5 NUMERICAL RESULTS

In this work, outer surface of FGPM thin-walled cylindrical shells is PZT_5A rich and the inner surface denotes BaTio3 rich. Temperature field varies in the thickness direction of cylindrical shell. The mechanical, thermal, and electrical constants of FGPM cylindrical shell are considered in Table 1. [27–29].

To validate the results of this work, the elastic coefficients of foundation equal to zero and the vibration frequencies of cylindrical shell is compared with the obtained results by Sheng and Wang [19]. As it is seen from Fig. 2, the results of this research are in a good agreement with the obtained results by [19]. The axial load and natural frequencies are nondimensionalized as $\lambda_N=N_0/N_1$ and $\lambda_\omega=\omega/\omega_1$, which ω_1, N_1 are the first natural frequency and buckling mode, respectively for $n=m=1$.

The influence of various values of the shear correction coefficient on the natural frequency of the piezoelectric-based FGM cylindrical shell is investigated in this study. A constant value of K_s=5/6 is commonly used for the isotropic material. A shear correction factor introduced by Mindlin and is equal to $\pi^2/12$ [23]. Timoshenko [30] presented a shear correction factor that depends on the Poisson ration $K_s = (5+\nu\cdot 5)/(6+\nu\cdot 5)$, the corresponding natural frequencies for three various shear correction factors (K_s) for FGPM cylindrical shells is presented in Table. 2. It can be concluded that by increasing shear correction factor, the natural frequencies of the FGPM cylindrical shell increases, also for higher circumferential wave numbers, the influence of shear correction factor on natural frequencies becomes more significant than lower circumferential wave numbers. Moreover, the difference between four cases for higher circumferential wave numbers increases.

Fig. 3 shows that by increasing the circumferential wave numbers, the nondimensional natural frequencies at first decreases and then increases. Also it is obvious that the frequency of system is dependent on the volume fraction exponent, in general by increasing the volume fraction exponent, nondimensional natural frequencies increases, also it is interesting that for wave number 5 the changes of nondimensional natural frequencies are negligible. From the results of Figs. 2 and 3 concluded that when the volume fraction exponent (β) is larger than 25, the natural frequencies are very close to those associated with β =100, so in this range, FGPM properties exhibit small variations and the cylindrical shell is BaTiO3 rich.

Table 1
The electro-thermo-mechanical constants of FGPM cylindrical shell

Material	*BaTio3*	*PZT_5A*	Material	*BaTio3*	*PZT_5A*	Material	*BaTio3*	*PZT_5A*
C_{11} (GPa)	166	99.201	C_{44} (GPa)	43	21.1	α_{11} (1/K)	11.3e-6	1.99e-6
C_{12} (GPa)	77	54.016	C_{55} (GPa)	43	21.1	α_{22} (1/K)	11.3e-6	1.99e-6
C_{13} (GPa)	78	50.778	C_{66} (GPa)	44.5	22.6	α_{33} (1/K)	11.3e-6	8.53e-6
C_{23} (GPa)	78	50.778	ζ_{11} ($C^2/N\cdot m^2$)	11.2e-9	1.53e-9	e_{15} (C/m^2)	11.6	12.322
C_{21} (GPa)	77	54.016	ζ_{22} ($C^2/N\cdot m^2$)	11.2e-9	1.53e-9	e_{31} (C/m^2)	-4.4	-7.209
C_{22} (GPa)	166	99.201	ζ_{33} ($C^2/N\cdot m^2$)	12.6e-9	1.50e-9	e_{32} (C/m^2)	-4.4	-7.209
C_{31} (GPa)	78	50.778	P_x ($C/m^2/K$)	-0.2e-6	-2.5e-5	e_{24} (C/m^2)	11.6	12.322
C_{32} (GPa)	78	50.778	P_θ ($C/m^2/K$)	-0.2e-6	-2.5e-5	e_{33} (C/m^2)	18.6	15.118
C_{33} (GPa)	162	86.856	P_z ($C/m^2/K$)	-0.2e-6	-2.5e-5	k (W/m/K)	2.72	0.72
ρ (kg/m^3)	5800	7750						

Table 2
The influence of shear correction factor (K_s) on natural frequencies of thin-walled piezoelectric-based FGM cylindrical shell
($m=1,\ R/h=100, DV=200v, \lambda_N=0.2, \beta=1, T_{io}=200k, K_w=5e6\ \ N/m^3, K_p=1e5\ \ N/m$)

K_s	Circumferential wave number (n)									
	1	2	3	4	5	6	7	8	9	10
0	2400.6316	1573.2351	1208.4050	1078.5826	1049.0071	1068.9600	1122.7313	1206.2355	1318.6397	1459.6084
$\pi^2/12$	2400.6316	1573.2351	1208.4051	1078.5832	1049.0093	1068.9666	1122.7476	1206.2697	1318.7036	1459.7176
5/6	2400.6316	1573.2351	1208.4051	1078.5832	1049.0093	1068.9667	1122.7478	1206.2701	1318.7044	1459.7190
$\frac{5+\nu\cdot 5}{6+\nu\cdot 5}$	2400.6316	1573.2351	1208.4051	1078.5832	1049.0094	1068.9670	1122.7485	1206.2715	1318.7070	1459.7235

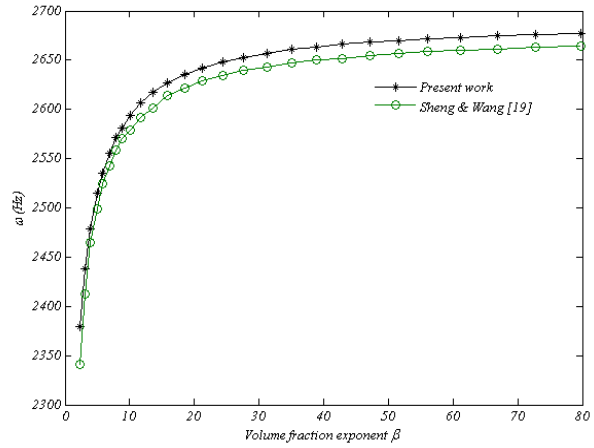

Fig. 2
Non-dimensional natural frequencies versus the volume fraction exponent for FGPM cylindrical shell without considering the elastic foundation (*m=1, n=1, L/R=2,R/h=100,ΔV=200v,* $N_0 = 850\ kN$, $T_{io} = 200k$, $K_w = 0$, $K_p = 0$).

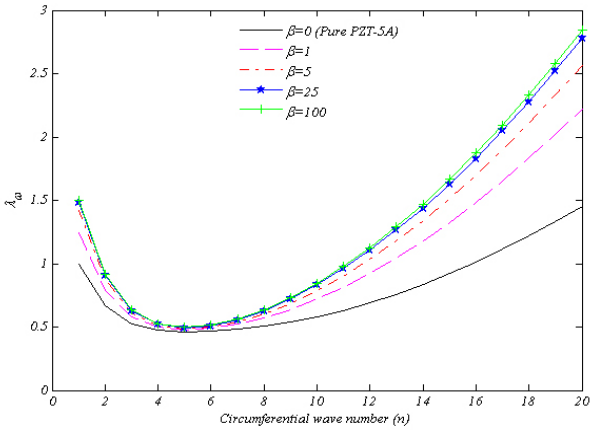

Fig. 3
Non-dimensional natural frequencies versus the circumferential wave number (*m=1, L/R=2, R/h=100, ΔV=200v,* $\lambda_N = 0.2, T_{io} = 200k, K_w = 5e6\ N/m^3$, $K_p = 1e5\ N/m$) for various volume fraction exponents.

In Fig. 4, the effects of radius to thickness ratio on the cylindrical shell natural frequencies are shown. It can be seen from the results that by increasing radius to thickness ratio, the natural frequencies decrease dramatically for wave number more than 4, and for less than 5, the effect of aspect ratio (*R/h*) on the natural frequencies is negligible. Fig. 5 shows the effect of length to radius ratio in the FGPM cylindrical shells. Unlike Fig. 4, increasing aspect ratio (*L/R*) causes a reduction of the natural frequencies for number wave less than 10, and for more than this value, the influence of aspect ratio on the natural frequencies are not significant. According to Fig. 6 for low temperature, increasing the temperature change between the inner and outer surfaces of FGPM cylindrical shells is caused to the natural frequency decreases. It is observed from this figure that the influence of the temperature change on the natural frequency is negligible for low temperature.

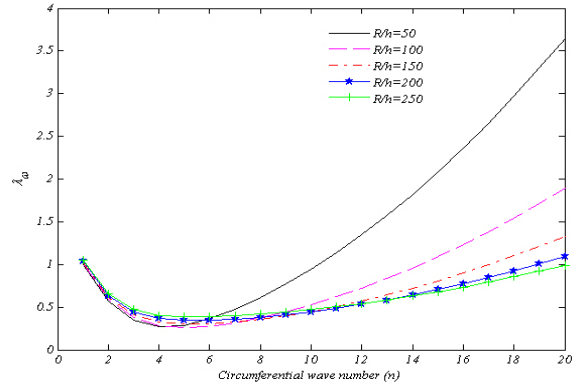

Fig. 4
Non-dimensional natural frequencies versus the circumferential wave number (*m=1, L/R=1, ΔV=200v,* $\lambda_N = 0.02, \beta = 1, T_{io} = 200k, K_w = 5e6\ N/m^3$,) $K_p = 1e5\ N/m$) for various radius to thickness ratios.

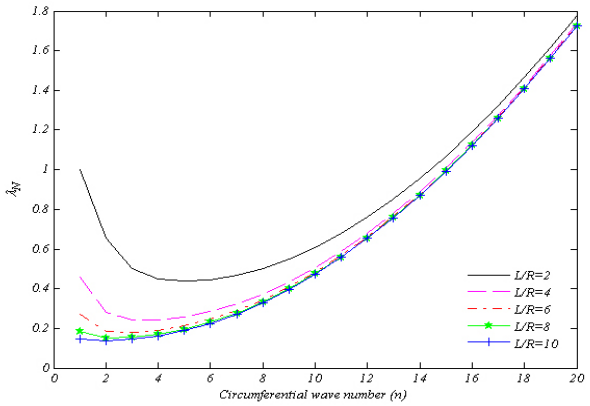

Fig. 5
Non-dimensional natural frequencies versus the circumferential wave number (*m=1, R/h=100, ΔV=200v,* $\lambda_N = 0.2, \beta = 1, T_{io} = 200k, K_w = 5e6\ N/m^3, K_p = 1e5\ N/m$) for various length to radius ratios.

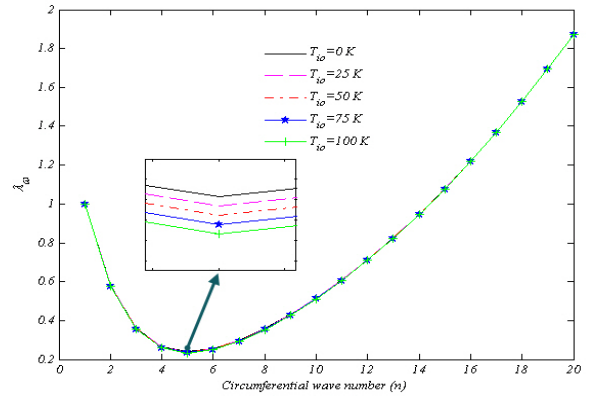

Fig. 6
Non-dimensional natural frequencies versus the circumferential wave number (*m=1, R/h=100, L/R=2, ΔV=200v,* $\lambda_N = 0.02, \beta = 1, K_w = 5e6\ N/m^3, K_p = 1e5\ N/m$) for various temperature changes.

The variation of natural frequencies versus the circumferential wave numbers is shown in Fig. 7. Also the effects of potential on the dimensionless natural frequencies determined that by increasing the electric potential between the inner and outer surfaces of cylindrical shells, the non-dimensional natural frequencies decrease.

In Fig. 8, the effect of axial force on the dimensionless natural frequencies is demonstrated. It is concluded from the results that the natural frequency increases with increasing the axial force, and this increase is more noticeable at the minimum of natural frequencies. In Fig. 9, the effect of Winkler coefficient on the natural frequencies is indicated. By increasing Winkler coefficient, the natural frequencies of cylindrical shells raised as a function of circumferential wave numbers. These changes are more significant at the minimum of natural frequencies.

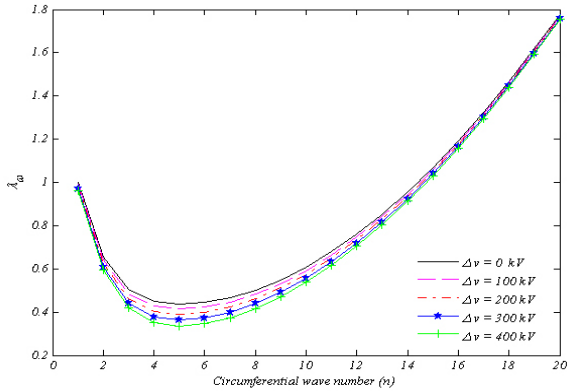

Fig. 7
Non-dimensional natural frequencies versus the circumferential wave number (*m=1, R/h=100, L/R=2,* $T_{io} = 200k, \lambda_N = 0.2, \beta = 1, K_w = 5e6\ N/m^3, K_p = 1e5\ N/m$) for various potential changes.

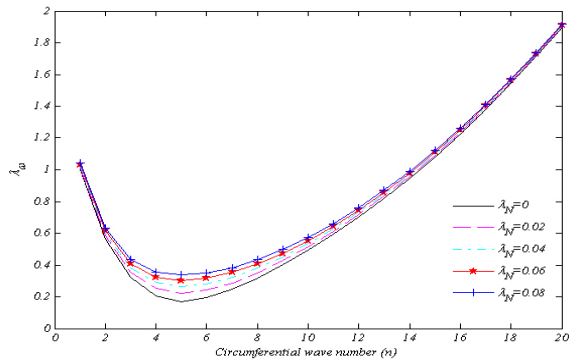

Fig. 8
Non-dimensional natural frequencies versus the circumferential wave number ($m=1$, $R/h=100$, $L/R=2$, $T_{io}=200k, DV=200v, \beta=1, K_w=5e6\ N/m^3, K_p=1e5\ N/m$) for various axial loadings.

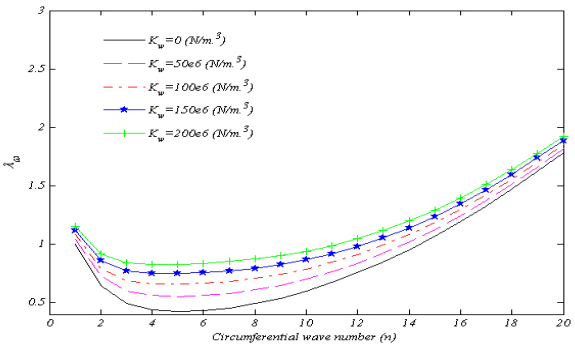

Fig. 9
Non-dimensional natural frequencies versus the circumferential wave number ($m=1$, $R/h=100$, $L/R=2$, $T_{io}=200k, DV=200v, \beta=1, \lambda_N=0.2, K_p=1e5\ N/m$) for various Winkler coefficients of elastic foundation.

Fig. 10 shows the variations of the natural frequencies versus the circumferential wave number. Also, the effects of Pasternak coefficient on the natural frequencies are presented in this figure. The dimensionless natural frequency of FGPM cylindrical shells increases with an increase in the Pasternak coefficient as a function of circumferential wave numbers. These changes are more considerable as the circumferential wave number became greater.

The non-dimensional buckling load (λ_N) versus the circumferential wave number for different Pasternak coefficients of elastic foundation is shown in Fig. 11. It is obvious that the critical buckling loads increases with increasing the Pasternak coefficient. Also the critical buckling loads increases rapidly as circumferential wave number (n) increases from 5 to 20. However, when n is <5, the critical buckling loads change very slowly, and the critical buckling loads are almost the same for different Pasternak coefficient of elastic foundation. Fig. 12 illustrates the non-dimensional buckling load (λN) versus the circumferential wave number for different Winkler coefficients of elastic foundation. The buckling load increases rapidly as circumferential wave number (n) increases when n is >10 . However, when n is <10, the buckling load changes slowly. In the Fig. 12, results show that by increasing Winkler coefficients of elastic foundation, the dimensionless critical buckling load increases. Also it is noteworthy that the effect of Winkler coefficients on the dimensionless critical buckling loads, are nearly equal for various circumferential wave number (n).

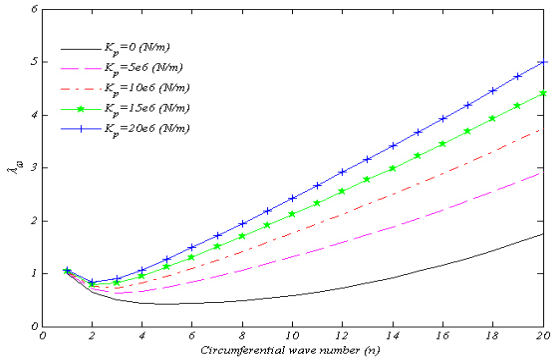

Fig. 10
Non-dimensional natural frequencies versus the circumferential wave number ($m=1$, $R/h=100$, $L/R=2$, $T_{io}=200k, DV=200v, \lambda_N=0.2, \beta=1, K_w=5e6\ N/m^3$)for various Pasternak coefficients of elastic foundation.

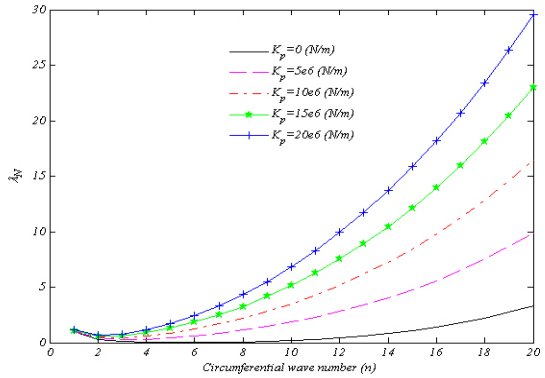

Fig.11
Non-dimensional buckling load versus the circumferential wave number (*m=1, R/h=100, L/R=2,* $T_{io}=200k$, $\Delta V=200v$, $\beta=1, K_w=5e6\ \ N/m^3$) for various Pasternak coefficient of elastic foundation.

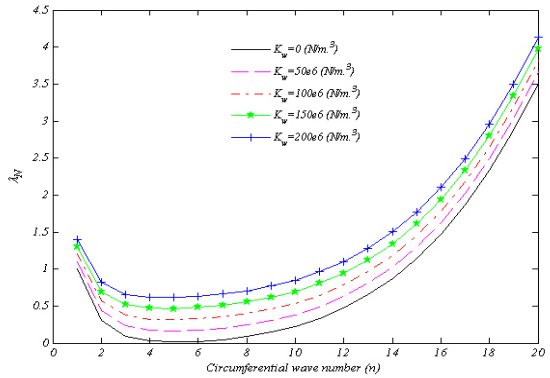

Fig.12
Non-dimensional buckling load versus the circumferential wave number (*m=1, R/h=100, L/R=2,* $T_{io}=200k$, $\Delta V=200v$, $\beta=1, K_p=1e5\ \ N/m$,) for various Winkler coefficients of elastic foundation.

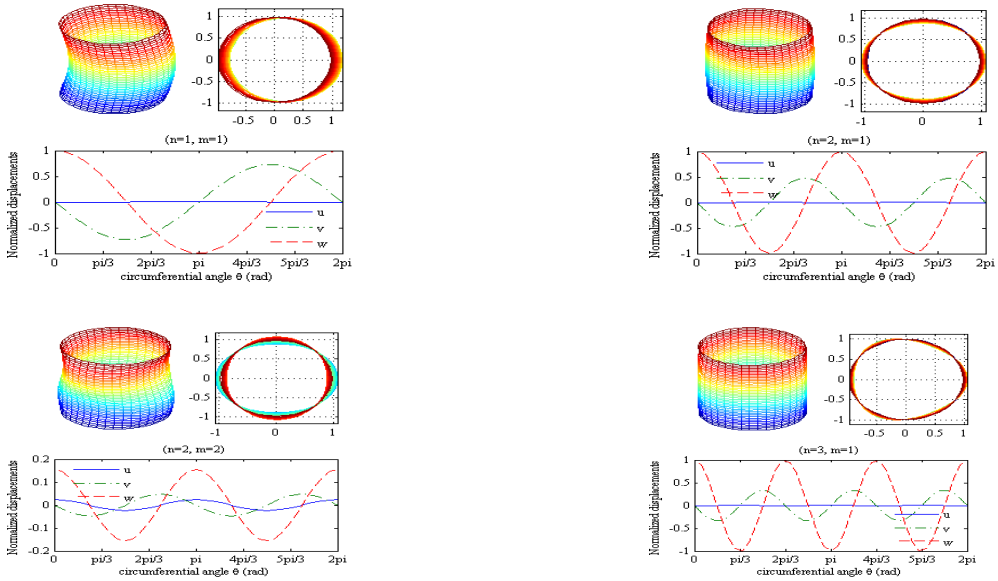

Fig. 13
Mode shapes versus circumferential angle (θ) with isometric and top view of deformed cylindrical shells for various *m* and *n* (*R/h=100, L/R=2,* $T_{io}=200k$, $\Delta V=200v$, $\beta=1, K_w=5e6\ \ N/m^3, K_p=1e5\ \ N/m$).

Fig. 13 presents the mode shapes versus circumferential angle (θ) for middle surface of the FGPM cylindrical shells at $x=L/2$. Also deformed cylindrical shells for various values of m and n are illustrated. The mode shapes corresponds to the first natural frequencies of cylindrical shells. This figure reveals that the distribution of the radial displacements (w) is more significant than circumferential (v) and longitudinal (u) displacements. The mode shapes corresponds to the first natural frequencies of cylindrical shells. It should be mentioned that the first natural frequency and buckling load do not necessarily correspond to the first possible mode.

6 CONCLUSIONS

This study considered the Pasternak foundation effects on the free vibration and buckling analysis for the thin-walled piezoelectric-based FGM cylindrical shells under electrical, thermal, and mechanical loadings. For this purpose, the effects of Winkler and Pasternak coefficients and other important parameters are investigated. Also dimensionless critical buckling loads and mode shapes of FGPM cylindrical shells are plotted. To drive the governing equations of motion, the Hamilton's principle, the Maxwell equation, and first-order shear deformation theory are used. The main results of this research can be listed as follows:

1. The dimensionless natural frequencies and buckling loads of FGPM cylindrical shells surrounded by the elastic foundation increase with increasing the Pasternak and Winkler elastic foundation coefficients. The effect of Pasternak coefficient on the non-dimensional critical buckling loads and natural frequencies increases by increasing circumferential wave numbers (n). However, the effect of Winkler coefficients on the dimensionless critical buckling loads and natural frequencies are more significant at the circumferential wave numbers which minimum of the natural frequencies occurred at them.
2. With increasing the volume fraction exponent of the FGPM cylindrical shells, the nondimensional natural frequencies increase, however for a specific circumferential wave number ($n=5$), the changes of nondimensional natural frequencies are negligible.
3. Increasing the length to radius ratio (L/R) and radius to thickness ratio (R/h) decrease the natural frequencies of FGPM cylindrical shells embedded on an elastic foundation.
4. The natural frequency of FGPM cylindrical shells decreases with an increase in the electric potential and temperature change between the inner and outer surfaces of cylindrical shells, and increasing the axial force increases the natural frequencies. Variation of the natural frequencies for different load conditions is more noticeable at the circumferential wave numbers which minimum of the natural frequencies occurred at them.
5. For the FGPM cylindrical shell resting on elastic foundation under combined loading, the distribution of the radial displacements (w) are more significant than circumferential (v) and longitudinal (u) displacements.
6. It can be concluded that by increasing shear correction factor, the natural frequencies of the FGPM cylindrical shell increases, also for higher circumferential wave numbers, the influence of shear correction factor on natural frequencies is more significant than lower circumferential wave numbers. Moreover, the difference between four cases for higher circumferential wave numbers increases.

ACKNOWLEDGMENTS

The authors would like to thank the referees for their valuable comments. They are also grateful to the University of Kashan for supporting this work by Grant No. 255941/5.

APPENDIX A

$$
\begin{aligned}
&\sigma_x = C_{11}\cdot\varepsilon_x + C_{12}\cdot\varepsilon_\theta + C_{13}\cdot\varepsilon_z - \left(C_{11}\cdot\alpha_{11} + C_{12}\cdot\alpha_{22} + C_{13}\cdot\alpha_{33}\right)\cdot T - e_{31}\cdot E_z,\\
&\sigma_\theta = C_{21}\cdot\varepsilon_x + C_{22}\cdot\varepsilon_\theta + C_{23}\cdot\varepsilon_z - \left(C_{21}\cdot\alpha_{11} + C_{22}\cdot\alpha_{22} + C_{23}\cdot\alpha_{33}\right)\cdot T - e_{32}\cdot E_z,\\
&\sigma_z = C_{31}\cdot\varepsilon_x + C_{32}\cdot\varepsilon_\theta + C_{33}\cdot\varepsilon_z - \left(C_{31}\cdot\alpha_{11} + C_{32}\cdot\alpha_{22} + C_{33}\cdot\alpha_{33}\right)\cdot T - e_{33}\cdot E_z,\\
&\tau_{\theta z} = C_{44}\cdot\gamma_{\theta z} - e_{24}\cdot E_\theta,\\
&\tau_{xz} = C_{55}\cdot\gamma_{xz} - e_{15}\cdot E_x,\\
&\tau_{x\theta} = Q_{66}\cdot\gamma_{x\theta},\\
&D_x = e_{15}\cdot\gamma_{xz} + \zeta_{11}\cdot E_x + P_x\cdot T,\\
&D_\theta = e_{24}\cdot\gamma_{\theta z} + \zeta_{22}\cdot E_\theta + P_\theta\cdot T,\\
&D_z = e_{31}\cdot\varepsilon_x + e_{32}\cdot\varepsilon_\theta + e_{33}\cdot\varepsilon_z + \zeta_{33}\cdot E_z + P_z\cdot T,
\end{aligned}
\tag{A.1}
$$

In this work, we consider thin-walled piezoelectric-based FGM cylindrical shell that this problem is the plane stress state ($\sigma_z = 0$), and then we have:

$$
\varepsilon_z = \frac{-C_{31}\,\varepsilon_x - C_{32}\,\varepsilon_\theta + \left(C_{31}\alpha_{11} + C_{32}\alpha_{22} + C_{33}\alpha_{33}\right)T + e_{33}\,E_z}{C_{33}},
\tag{A.2}
$$

Substituting Eq. (A.2) in the constitutive equations of a piezoelectric cylindrical shell yields:

$$
\begin{aligned}
\sigma_x &= \left(C_{11} - \frac{C_{13}\cdot C_{31}}{C_{33}}\right)\varepsilon_x + \left(C_{12} - \frac{C_{13}\cdot C_{32}}{C_{33}}\right)\varepsilon_\theta - \left(\left(C_{11} - \frac{C_{13}C_{31}}{C_{33}}\right)\alpha_{11} + \left(C_{12} - \frac{C_{13}C_{32}}{C_{33}}\right)\alpha_{22}\right)T + \left(\frac{C_{13}}{C_{33}}e_{33} - e_{31}\right)\cdot E_z,\\
\sigma_\theta &= \left(C_{21} - \frac{C_{23}\cdot C_{31}}{C_{33}}\right)\varepsilon_x + \left(C_{22} - \frac{C_{23}\cdot C_{32}}{C_{33}}\right)\varepsilon_\theta - \left(\left(C_{21} - \frac{C_{23}C_{31}}{C_{33}}\right)\alpha_{11} + \left(C_{22} - \frac{C_{23}C_{32}}{C_{33}}\right)\alpha_{22}\right)T + \left(\frac{C_{23}}{C_{33}}e_{33} - e_{32}\right)\cdot E_z,\\
D_z &= \left(e_{31} - \frac{C_{31}}{C_{33}}e_{33}\right)\varepsilon_x + \left(e_{32} - \frac{C_{32}}{C_{33}}e_{33}\right)\varepsilon_\theta - \left(\zeta_{33} + \frac{e_{33}}{C_{33}}e_{33}\right)E_z + \left(P_z + \frac{C_{31}\alpha_{11} + C_{32}\alpha_{22} + C_{33}\alpha_{33}}{C_{33}}e_{33}\right)\cdot T,
\end{aligned}
\tag{A.3}
$$

Thus using Eqs. (A.3) , one can define the equivalent values of material properties such as mechanical, electrical, and thermal for plane stress state:

$$
\begin{aligned}
&C_{11e} = C_{11} - \frac{C_{13}C_{13}}{C_{33}},\quad C_{12e} = C_{12} - \frac{C_{13}C_{23}}{C_{33}},\quad C_{22e} = C_{22} - \frac{C_{23}C_{23}}{C_{33}},\quad C_{44e} = C_{44},\quad C_{55e} = C_{55},\quad C_{66e} = C_{66},\\
&e_{15e} = e_{15},\quad e_{31e} = e_{31} - \frac{C_{13}e_{33}}{C_{33}},\quad e_{32e} = e_{32} - \frac{C_{23}e_{33}}{C_{33}},\quad e_{24e} = e_{24},\\
&P_{xe} = P_x,\quad P_{\theta e} = P_\theta,\quad P_{ze} = P_z + \frac{e_{33}}{C_{33}}\cdot(C_{31}\alpha_{11} + C_{32}\alpha_{22} + C_{33}\alpha_{33}),\\
&\zeta_{11e} = \zeta_{11},\quad \zeta_{22e} = \zeta_{22},\quad \zeta_{33e} = \zeta_{33} + \frac{e_{33}e_{33}}{C_{33}},\\
&\alpha_{11e} = \alpha_{11},\quad \alpha_{22e} = \alpha_{22},
\end{aligned}
\tag{A.4}
$$

APPENDIX B

$$B_{11}=A_{11}\frac{\partial^2}{\partial x^2}+\frac{A_{66}}{R^2}\frac{\partial^2}{\partial\theta^2},\quad B_{12}=\frac{A_{12}+A_{66}}{R}\frac{\partial^2}{\partial\theta\,\partial x},\quad B_{13}=\frac{A_{12}}{R}\frac{\partial}{\partial x},\quad B_{14}=A'_{11}\frac{\partial^2}{\partial x^2}+\frac{A'_{66}}{R^2}\frac{\partial^2}{\partial\theta^2},$$

$$B_{15}=\frac{A'_{12}+A'_{66}}{R}\frac{\partial^2}{\partial\theta\,\partial x},\quad \mathrm{B}_{16}=Q_{E12}\frac{\partial}{\partial x},\quad B_1=-\frac{\partial N_x^T}{\partial x}+Q_{E11}\frac{\partial V}{\partial x},$$

$$B_{21}=\frac{A_{12}+A_{66}}{R}\frac{\partial^2}{\partial\theta\,\partial x},\quad B_{22}=A_{66}\frac{\partial^2}{\partial x^2}+\frac{A_{22}}{R^2}\frac{\partial^2}{\partial\theta^2}-\frac{k_sA_{44}}{R^2}+\left(N_0-N_x^T+N_x^P\right)\frac{\partial^2}{\partial x^2},$$

$$B_{23}=\frac{A_{22}+k_sA_{44}}{R^2}\frac{\partial}{\partial\theta},\quad \mathrm{B}_{24}=\frac{A'_{12}+A'_{66}}{R}\frac{\partial^2}{\partial\theta\,\partial x},\quad B_{25}=A'_{66}\frac{\partial^2}{\partial x^2}+\frac{A'_{22}}{R^2}\frac{\partial^2}{\partial\theta^2}+\frac{k_sA_{44}}{R^2},$$

$$B_{26}=\frac{\left(Q_{T12}+Q_{E22}\right)}{R}\frac{\partial}{\partial\theta},\quad \mathrm{B}_2=\frac{Q_{T11}+Q_{E21}}{R}\frac{\partial V}{\partial\theta}-\frac{1}{R}\frac{\partial N_\theta^T}{\partial\theta},$$

$$B_{31}=-\frac{A_{12}}{R}\frac{\partial}{\partial x},\quad B_{32}=-\frac{A_{22}+k_sA_{44}}{R^2}\frac{\partial}{\partial\theta},$$

$$B_{33}=\left(k_sA_{55}+k_p\right)\frac{\partial^2}{\partial x^2}+\frac{\left(k_sA_{44}+k_p\right)}{R^2}\frac{\partial^2}{\partial\theta^2}-\frac{A_{22}}{R^2}+\left(N_0-N_x^T+N_x^P\right)\frac{\partial^2}{\partial x^2}-\mathrm{k}_w,$$

$$B_{34}=k_sA_{55}\frac{\partial}{\partial x}-\frac{A'_{21}}{R}\frac{\partial}{\partial x},\quad B_{35}=\frac{k_sA_{44}}{R}\frac{\partial}{\partial\theta}-\frac{A'_{22}}{R^2}\frac{\partial}{\partial\theta},$$

$$B_{36}=-\frac{1}{R}Q_{E11}+\frac{Q_{T12}}{R}\frac{\partial^2}{\partial\theta^2}+Q_{T22}\frac{\partial^2}{\partial x^2},\ B_3=-\frac{1}{R}Q_{E21}V+\frac{1}{R}N_\theta^T+\frac{Q_{T11}}{R}\frac{\partial^2V}{\partial\theta^2}+Q_{T21}\frac{\partial^2V}{\partial x^2},$$

$$B_{41}=A'_{11}\frac{\partial^2}{\partial x^2}+\frac{A'_{66}}{R^2}\frac{\partial^2}{\partial\theta^2},\quad \mathrm{B}_{42}=\frac{A'_{12}+A'_{66}}{R}\frac{\partial^2}{\partial\theta\,\partial x},\quad B_{43}=-k_sA_{55}\frac{\partial}{\partial x}+\frac{A'_{21}}{R}\frac{\partial}{\partial x},$$

$$B_{44}=A''_{11}\frac{\partial^2}{\partial x^2}+\frac{A''_{66}}{R^2}\frac{\partial^2}{\partial\theta^2}-k_sA_{55},\quad \mathrm{B}_{45}=\frac{A''_{12}+A''_{66}}{R}\frac{\partial^2}{\partial\theta\,\partial x},\tag{B.1}$$

$$B_{46}=\left(Q_{M12}-Q_{T22}\right)\frac{\partial}{\partial x},\quad B_4=\left(Q_{M11}-Q_{T21}\right)\frac{\partial V}{\partial x}-\frac{\partial M_x^T}{\partial x},$$

$$B_{51}=\frac{A'_{12}+A'_{66}}{R}\frac{\partial^2}{\partial\theta\,\partial x},\quad B_{52}=A'_{66}\frac{\partial^2}{\partial x^2}+\frac{A'_{22}}{R^2}\frac{\partial^2}{\partial\theta^2}+\frac{k_sA_{44}}{R^2},\quad B_{53}=\frac{k_sA_{44}}{R}\frac{\partial}{\partial\theta}-\frac{A'_{22}}{R^2}\frac{\partial}{\partial\theta},$$

$$\mathrm{B}_{54}=\frac{A''_{12}+A''_{66}}{R}\frac{\partial^2}{\partial\theta\,\partial x},\quad B_{55}=A''_{66}\frac{\partial^2}{\partial x^2}+\frac{A''_{22}}{R^2}\frac{\partial^2}{\partial\theta^2}-k_sA_{44},B_{56}=\left(\frac{Q_{M22}}{R}-Q_{T12}\right)\frac{\partial}{\partial\theta},$$

$$B_5=\left(\frac{Q_{M21}}{R}-Q_{T11}\right)\frac{\partial V}{\partial\theta}-\frac{1}{R}\frac{\partial M_\theta^T}{\partial\theta},$$

$$\mathrm{B}_{61}=\int_{-h/2}^{h/2}\frac{e_{31e}}{R}dz\frac{\partial}{\partial x},\quad \mathrm{B}_{62}=\int_{-h/2}^{h/2}\frac{e_{32e}}{R^2}dz\frac{\partial}{\partial\theta},\quad \mathrm{B}_{63}=\int_{-h/2}^{h/2}e_{15e}dz\frac{\partial^2}{\partial x^2}+\int_{-h/2}^{h/2}\frac{e_{24e}}{R^2}dz\frac{\partial^2}{\partial\theta^2}\quad+\int_{-h/2}^{h/2}\frac{e_{32e}}{R^2}dz,$$

$$B_{64}=\int_{-h/2}^{h/2}\left(e_{15e}+e_{31e}+\frac{e_{13e}}{R}z\right)dz\frac{\partial}{\partial x},\quad B_{65}=\int_{-h/2}^{h/2}\left(\frac{e_{24e}}{R}+\frac{e_{32e}}{R}+\frac{e_{32e}}{R^2}z\right)dz\frac{\partial}{\partial\theta},$$

$$B_{66}=-\int_{-h/2}^{h/2}\zeta_{22e}P(z)dz\frac{\partial^2}{\partial x^2}-\int_{-h/2}^{h/2}\frac{\zeta_{22e}P(z)}{R(R+z)}dz\frac{\partial^2}{\partial\theta^2}-2\int_{-h/2}^{h/2}\zeta_{33e}dz-2\int_{-h/2}^{h/2}\frac{\zeta_{33e}}{R}zdz,$$

$$B_6=-2\int_{-h/2}^{h/2}\frac{\zeta_{22e}}{R(R+z)\mathrm{h}}zdz\frac{\partial^2V}{\partial\theta^2}-2\int_{-h/2}^{h/2}\frac{\zeta_{33e}}{Rh}dzV-2\int_{-h/2}^{h/2}\frac{\zeta_{11e}}{h}zdz\frac{\partial^2V}{\partial x^2}+\int_{-h/2}^{h/2}\left(\frac{\partial T}{\partial x}P_{xe}+\frac{1}{R}\frac{\partial T}{\partial\theta}P_{\theta e}+\frac{\partial T}{\partial z}P_{ze}+\frac{T}{R}P_{ze}\right)dz.$$

$$
\begin{aligned}
&Q_{M22}=2\int_{-h/2}^{h/2}e_{32e}z^2dz,\quad Q_{M21}=2\int_{-h/2}^{h/2}\frac{e_{32e}}{h}zdz,\quad Q_{M12}=2\int_{-h/2}^{h/2}e_{31e}z^2dz,\quad Q_{M11}=2\int_{-h/2}^{h/2}\frac{e_{31e}}{h}zdz,\\
&Q_{E11}=2\int_{-h/2}^{h/2}\frac{e_{31e}}{h}dz,\quad Q_{E12}=2\int_{-h/2}^{h/2}e_{31e}zdz,\quad Q_{E21}=2\int_{-h/2}^{h/2}\frac{e_{32e}}{h}dz,\quad Q_{E22}=2\int_{-h/2}^{h/2}e_{32e}zdz,\\
&Q_{T11}=2\,k_s\int_{-h/2}^{h/2}\frac{e_{24e}}{(R+z)h}zdz,\quad Q_{T22}=k_s\int_{-h/2}^{h/2}e_{15e}P(z)dz,\quad Q_{T21}=2\,k_s\int_{-h/2}^{h/2}\frac{e_{15e}}{h}zdz,\\
&Q_{T12}=-k_s\int_{-h/2}^{h/2}\frac{e_{24e}P(z)}{(R+z)}dz,
\end{aligned}
\tag{B.2}
$$

$$
\begin{aligned}
&p(z)=z^2-\left(\frac{h}{2}\right)^2,\quad \left(A_{ij},A'_{ij},A''_{ij}\right)=\int_{-h/2}^{h/2}C_{ije}\left(1,z,z^2\right)dz\quad (i,j=1,2,4,5,6),\\
&\begin{Bmatrix}N_x^T\\N_\theta^T\end{Bmatrix}=\int_{-h/2}^{h/2}\begin{Bmatrix}C_{11e}\alpha_{11e}+C_{12e}\alpha_{22e}\\C_{12e}\alpha_{11e}+C_{22e}\alpha_{22e}\end{Bmatrix}T(z)dz\quad,\quad \begin{Bmatrix}M_x^T\\M_\theta^T\end{Bmatrix}=\int_{-h/2}^{h/2}\begin{Bmatrix}C_{11e}\alpha_{11e}+C_{12e}\alpha_{22e}\\C_{12e}\alpha_{11e}+C_{22e}\alpha_{22e}\end{Bmatrix}T(z)zdz,\\
&\begin{Bmatrix}N_x^P\\N_\theta^P\end{Bmatrix}=2\int_{-h/2}^{h/2}\begin{bmatrix}\frac{e_{31e}}{h} & e_{31e}z\\ \frac{e_{32e}}{h} & e_{32e}z\end{bmatrix}dz\cdot\begin{Bmatrix}V\\\psi\end{Bmatrix}\quad,\quad \begin{Bmatrix}M_x^P\\M_\theta^P\end{Bmatrix}=2\int_{-h/2}^{h/2}\begin{bmatrix}\frac{e_{31e}}{h} & e_{31e}z\\ \frac{e_{32e}}{h} & e_{32e}z\end{bmatrix}zdz\cdot\begin{Bmatrix}V\\\psi\end{Bmatrix},
\end{aligned}
\tag{B.3}
$$

APPENDIX C

$$
\begin{aligned}
&T_{11}=A_{11}\lambda_m^2+\frac{A_{66}}{R^2}n^2,\quad T_{12}=-\frac{A_{12}+A_{66}}{R}\lambda_m n,\quad T_{13}=-\frac{A_{12}}{R}\lambda_m,\quad T_{14}=A'_{11}\lambda_m^2+\frac{A'_{66}}{R^2}n^2,\\
&T_{15}=-\frac{A'_{12}+A'_{66}}{R}\lambda_m\,\mathrm{n},\quad T_{16}=-Q_{E12}\lambda_m,\quad T_{21}=-\frac{A_{12}+A_{66}}{R}\lambda_m\,\mathrm{n},\\
&T_{22}=A_{66}\lambda_m^2+\frac{A_{22}}{R^2}n^2+\frac{k_sA_{44}}{R^2}+\left(N_0-T_{io}N_T+VN_V\right)\lambda_m^2,\quad T_{23}=\frac{A_{22}+k_sA_{44}}{R^2}n,\quad T_{24}=-\frac{A'_{12}+A'_{66}}{R}\lambda_m\,\mathrm{n},\\
&T_{25}=A'_{66}\lambda_m^2+\frac{A'_{22}}{R^2}n^2-\frac{k_sA_{44}}{R^2},\quad T_{26}=\frac{\left(Q_{T12}+Q_{E22}\right)}{R}n,\quad T_{31}=-\frac{A_{12}}{R}\lambda_m,\quad T_{32}=\frac{A_{22}+k_sA_{44}}{R^2}n,\\
&T_{33}=\left(k_sA_{55}+k_p\right)\lambda_m^2+\frac{\left(k_sA_{44}+k_p\right)}{R^2}n^2+\left(N_0-T_{io}N_T+VN_V\right)\lambda_m^2-\frac{A_{22}}{R^2}-k_w,\quad T_{34}=\left(k_sA_{55}-\frac{A'_{21}}{R}\right)\lambda_m,\\
&T_{35}=\left(-\frac{k_sA_{44}}{R}+\frac{A'_{22}}{R^2}\right)n,\quad T_{36}=-\frac{1}{R}Q_{E11}+\frac{Q_{T12}}{R}n^2+Q_{T22}\lambda_m^2,\quad T_{41}=A'_{11}\lambda_m^2+\frac{A'_{66}}{R^2}n^2,\\
&T_{42}=-\frac{A'_{12}+A'_{66}}{R}\lambda_m\,\mathrm{n},\quad T_{43}=k_sA_{55}\lambda_m-\frac{A'_{21}}{R}\lambda_m,\quad T_{44}=A''_{11}\lambda_m^2+\frac{A''_{66}}{R^2}n^2+k_sA_{55},\\
&T_{45}=-\frac{A''_{12}+A''_{66}}{R}\lambda_m\,\mathrm{n},\quad T_{46}=\left(-Q_{M12}+Q_{T22}\right)\lambda_m,\quad T_{51}=-\frac{A'_{12}+A'_{66}}{R}\lambda_m\,\mathrm{n},\\
&T_{52}=A'_{66}\lambda_m^2+\frac{A'_{22}}{R^2}n^2-\frac{k_sA_{44}}{R^2},\quad T_{53}=-\frac{k_sA_{44}}{R}n+\frac{A'_{22}}{R^2}n,\quad T_{54}=-\frac{A''_{12}+A''_{66}}{R}\lambda_m\,\mathrm{n},\\
&T_{55}=A''_{66}\lambda_m^2+\frac{A''_{22}}{R^2}n^2+k_sA_{44},\quad T_{56}=\left(\frac{Q_{M22}}{R}-Q_{T12}\right)n,\quad T_{61}=-\int_{-h/2}^{h/2}\frac{e_{31e}}{R}dz\lambda_m,\\
&T_{62}=\int_{-h/2}^{h/2}\frac{e_{32e}}{R^2}dzn,\quad T_{63}=-\int_{-h/2}^{h/2}e_{15e}dz\lambda_m^2-\int_{-h/2}^{h/2}\frac{e_{24e}}{R^2}dzn^2+\int_{-h/2}^{h/2}\frac{e_{32e}}{R^2}dz\,,\\
&T_{64}=-\int_{-h/2}^{h/2}\left(e_{15e}+e_{31e}+\frac{e_{13e}}{R}z\right)dz\lambda_m,\quad T_{65}=\int_{-h/2}^{h/2}\left(\frac{e_{24e}}{R}+\frac{e_{32e}}{R}+\frac{e_{32e}}{R^2}z\right)dz\cdot n,\\
&T_{66}=\int_{-h/2}^{h/2}\zeta_{22e}P(z)dz\lambda_m^2+\int_{-h/2}^{h/2}\frac{\zeta_{22e}P(z)}{R(R+z)}dzn^2\;-2\int_{-h/2}^{h/2}\zeta_{33e}dz-2\int_{-h/2}^{h/2}\frac{\zeta_{33e}}{R}zdz,
\end{aligned}
\tag{C.1}
$$

$$
\begin{aligned}
&X=\int_{-h/2}^{h/2}\int_{-h/2}^{z}\frac{C_{11e}\alpha_{11e}+C_{12e}\alpha_{22e}}{K(\tau)\cdot\tau}\cdot d\tau\cdot dz,\quad Y=\int_{-h/2}^{h/2}\frac{1}{K(\tau)\cdot\tau}\cdot d\tau,\\
&N_T=\int_{-h/2}^{h/2}\left(C_{11e}\alpha_{11e}+C_{12e}\alpha_{22e}\right)dz-X/Y,\quad \mathrm{N}_V=2\int_{-h/2}^{h/2}\frac{e_{31e}}{h}dz,\\
&N_T=\int_{-h/2}^{h/2}\left(C_{11e}\alpha_{11e}+C_{12e}\alpha_{22e}\right)dz-\frac{\int_{-h/2}^{h/2}\int_{-h/2}^{z}\frac{C_{11e}\alpha_{11e}+C_{12e}\alpha_{22e}}{K(\tau)\cdot\tau}\cdot d\tau\cdot dz}{\int_{-h/2}^{h/2}\frac{1}{K(\tau)\cdot\tau}\cdot d\tau},\quad \mathrm{N}_V=2\int_{-h/2}^{h/2}\frac{e_{31e}}{h}dz,
\end{aligned}
\tag{C.2}
$$

where N_v, N_T are temperature, and potential coefficients, respectively.

APPENDIX D

$$
\left[K_{11}\right]=\begin{bmatrix}T_{11}&T_{12}&T_{13}&T_{14}&T_{15}\\T_{21}&T_{22}&T_{23}&T_{24}&T_{25}\\T_{31}&T_{32}&T_{33}&T_{34}&T_{35}\\T_{41}&T_{42}&T_{43}&T_{44}&T_{45}\\T_{51}&T_{52}&T_{53}&T_{54}&T_{55}\end{bmatrix},\quad \left[K\right]_N=\begin{bmatrix}0&0&0&0&0\\0&-\lambda_m^2&0&0&0\\0&0&-\lambda_m^2&0&0\\0&0&0&0&0\\0&0&0&0&0\end{bmatrix},
$$

$$
\left[K\right]_T=-N_T\left[K\right]_N,\quad \left[K\right]_V=N_V\left[K\right]_N,\quad K_{22}=T_{66},
$$

$$
\left\{K_{12}\right\}^T=\left\{T_{16}\quad T_{26}\quad T_{36}\quad T_{46}\quad T_{56}\right\},
$$

$$
\left[K_{21}\right]=\left\{T_{61}\quad T_{62}\quad T_{63}\quad T_{64}\quad T_{65}\right\},
$$

$$
\left\{F\right\}=\left\{B_{mn}^1(t)\quad B_{mn}^2(t)\quad B_{mn}^3(t)\quad B_{mn}^4(t)\quad B_{mn}^5(t)\right\}^T-\frac{\left\{K_{12}\right\}^T}{K_{22}}L_{mn}^6(t)
$$

REFERENCES

[1] Yamanouchi M., Koizumi M., Hirai T., Shiota I., 1990, Functionally gradient materials, *Proceedings of the first International Symposium on Functionally Gradient Materials* 327-332.

[2] Koizumi M., 1993, The concept of FGM ceramic transactions, *Functionally Graded Materials* **34**: 3-10.

[3] Pasternak P., 1954, *On a New Method of Analysis of an Elastic Foundation by Means of Two Foundation Constants*, Gosudarstvenneo Izdatelstvo Literaturi po Stroitelstvu Arkhitekture, Moscow, USSR.

[4] Loy CT., Lam KY., Reddy JN., 1999, Vibration of functionally graded cylindrical shells, *International Journal of Mechanical Sciences* **41**: 309-324.

[5] Pradhan SC., Loy CT., Lam KY., Reddy JN., 2000, Vibration characteristics of functionally graded cylindrical shells under various boundary conditions, *Applied Acoustics* **61**: 111-129.

[6] Najafizadeh M.M., Isvandzibaei M.R., 2007, Vibration of functionally graded cylindrical shells based on higher order shear deformation plate theory with ring support, *Acta Mechanica* **191**: 75-91.

[7] Shah AG., Mahmood T., Naeem MN., Iqbal Z., Arshad SH., 2009, Vibrations of functionally graded cylindrical shells based on elastic foundations, *Acta Mechanica* **211**: 293-307.

[8] Bhangale RK., Ganesan N., 2005, Free vibration studies of simply supported non-homogeneous functionally graded magneto-electro-elastic finite cylindrical shells, *Journal of Sound and Vibration* **288**: 412-422.

[9] Kadoli R., Ganesan N., 2006, Buckling and free vibration analysis of functionally graded cylindrical shells subjected to a temperature-specified boundary condition, *Journal of Sound and Vibration* **289**: 450-480.

[10] Malekzadeh P., Heydarpour Y., 2012, Free vibration analysis of rotating functionally graded cylindrical shells in thermal environment, *Composite Structures* **94**: 2971-2981.

[11] Ebrahimi MJ., Najafizadeh MM., 2014, Free vibration analysis of two-dimensional functionally graded cylindrical shells, *Applied Mathematical Modelling* **38**: 308-324.
[12] Sheng GG., Wang X., 2013, Nonlinear vibration control of functionally graded laminated cylindrical shells, *Composites Part B: Engineering* **52**: 1-10.
[13] Du C., Li Y., 2013, Nonlinear resonance behavior of functionally graded cylindrical shells in thermal environments, *Composite Structures* **102**: 164-174.
[14] Sofiyev AH., Kuruoglu N., 2013, Torsional vibration and buckling of the cylindrical shell with functionally graded coatings surrounded by an elastic medium, *Composites Part B: Engineering* **45**: 1133-1142.
[15] Sheng GG., Wang X., 2013, An analytical study of the non-linear vibrations of functionally graded cylindrical shells subjected to thermal and axial loads, *Composite Structures* **97**: 261-268.
[16] Rafiee M., Mohammadi M., Aragh BS., Yaghoobi H., 2013, Nonlinear free and forced thermo-electro-aero-elastic vibration and dynamic response of piezoelectric functionally graded laminated composite shells, *Composite Structures* **103**: 188-196.
[17] Ghorbanpour Arani A., Bakhtiari R., Mohammadimehr M., Mozdianfard M.R., 2011, Electromagnetomechanical responses of a radially polarized rotating functionally graded piezoelectric shaft, *Turkish Journal of Engineering & Environmental Sciences* **36**(1): 33-44.
[18] Khoshgoftar MJ., Ghorbanpour Arani A., Arefi M., 2009, Thermoelastic analysis of a thick walled cylinder made of functionally graded piezoelectric material, *Smart Material Structures* **18**: 115007-115015.
[19] Sheng GG., Wang X., 2010, Thermoelastic vibration and buckling analysis of functionally graded piezoelectric cylindrical shells, *Applied Mathematical Modelling* **34**: 2630-2643.
[20] Fernandes A., Pouget J., 2006, Structural response of composite plates equipped with piezoelectric actuators, *Computer and Structures* **84**: 1459-1470.
[21] Bagherizadeh E., Kiani Y., Eslami M.R., 2011, Mechanical buckling of functionally graded material cylindrical shells surrounded by Pasternak elastic foundation, *Composite Structures* **93**: 3063-3071.
[22] Pouresmaeeli S., Fazelzadeh S.A., Ghavanloo E., 2012, Exact solution for nonlocal vibration of double-orthotropic nanoplates embedded in elastic medium, *Composites Part B: Engineering* **43**: 3384-3390.
[23] Jafari A.A., Khalili S.M.R., Azarafza R., 2005, Transient dynamic response of composite circular cylindrical shells under radial impulse load and axial compressive loads, *Thin-Walled Structures* **43**: 1763-1786.
[24] Dong K., Wang X., 2007, Wave propagation characteristics in piezoelectric cylindrical laminated shells under large deformation, *Composite Structures* **77**: 171-181.
[25] Ghorbanpour Arani A., Fesharaki J.J., Mohammadimehr M., Golabi S., 2010, Electro-magneto-thermo-mechanical behaviors of a radially polarized FGPM thick hollow sphere, *Journal of Solid Mechanics* **2**: 305-315.
[26] Heyliger P., 1997, A note on the static behavior of simply supported laminated piezoelectric cylinders, *International Journal of Solid and Structures* **34**: 3781-3794.
[27] He Y., 2004, Heat capacity, thermal conductivity, and thermal expansion of barium titanate-based ceramics, *Thermochimica Acta* **419**: 135-141.
[28] Ramirez F., Heyliger P.R., Pan E., 2006, Free vibration response of two-dimensional magneto-electro-elastic laminated plates, *Journal of Sound and Vibrations* **292**: 626-644.
[29] Arani A.G., Jafarzadeh Jazi A., Abdollahian M., Mozdianfard M.R., Mohammadimehr M., Amir S., Exact solution for electrothermoelastic behaviors of a radially polarized FGPM Rotating Disk, *Journal of Solid Mechanics* **3**: 244-257.
[30] Timoshenko S.P., 1922, On the transverse vibrations of bars of uniform cross-section, *Philosophical Magazine* **43**: 125-131.